Nafta-Gaz 2026, vol. 82, no. 4, pp. 371–386, DOI: 10.18668/NG.2026.04.05

Dynamic Assessment and Control of Wax Deposition Risks in Multiphase Crude Oil Pipeline Networks

Dynamiczna ocena i kontrola ryzyka wytrącania się parafiny w sieciach rurociągów do wielofazowego transportu ropy naftowej

Huaixin Zhang[1*], Ziqi Zhang[2*], Tengjiao He[2*], Kexi Liao[2], Guoxi He[2], Min Qin[2], Yuhan Liu[3]

[1] *School of computer science and software engineering, Southwest Petroleum University, Chengdu, 610500, China*
[2] *Petroleum Engineering School, Southwest Petroleum University, Chengdu, 610500, China*
[3] *Sichuan Natural Gas Sales Center, Sinopec Natural Gas Company, Chengdu, 610011, China*
[*] *Corresponding authors*

ABSTRACT: During unheated transport, high-water-cut and high-pour-point crude oil is prone to blockage because of wax crystallization, viscosity increase, and oil-water emulsification. Therefore, defining an appropriate inlet heating temperature is crucial. However, the critical flow temperature under flowing conditions remains unclear for crude oil with different compositions, and a quantitative method for flow safety evaluation is lacking. Consequently, dynamic and precise temperature control over the full operational cycle cannot be achieved. First, experimental data from dynamic critical-temperature tests were used to predict the critical flow temperature under variable operating conditions using the Light Gradient Boosting Machine (LightGBM) algorithm. A corresponding safety indicator was established. Subsequently, the critical inlet temperature was determined using a coupled flow model of the pipeline network. A novel safety assessment criterion, based on "failure probability and consequence severity", was proposed. This method enables accurate evaluation of the flow safety status of crude oil pipelines. The approach supports safe operation of oilfield pipeline networks while reducing energy consumption and improving economic efficiency. The results show that the proposed model predicts the critical flow temperature of crude oil with an average error of 6.4%, indicating high accuracy. The evaluation method is applicable under variable operating conditions. Applying this evaluation to a pipeline network enabled a full-cycle dynamic heating scheme, reducing natural gas consumption by 57.7%.

Keywords: crude oil flow, oilfield transmission pipeline network, flow process safety assessment, operation strategy.

STRESZCZENIE: Podczas transportu bez podgrzewania ropy naftowej o dużej zawartości wody i wysokiej temperaturze krzepnięcia rurociągi są narażone na powstawanie zatorów wskutek krystalizacji parafiny, wzrostu lepkości oraz tworzenie emulsji ropa–woda. Dlatego też kluczowe znaczenie ma określenie odpowiedniej temperatury podgrzewania na wlocie. W przypadku ropy naftowej o różnym składzie krytyczna temperatura przepływu w warunkach dynamicznych nie została jednak dotychczas jednoznacznie określona, a ponadto brakuje ilościowej metody oceny bezpieczeństwa przepływu. Uniemożliwia to dynamiczne i precyzyjne sterowanie temperaturą w całym cyklu eksploatacyjnym. W pierwszym etapie wykorzystano dane doświadczalne uzyskane w dynamicznych badaniach temperatury krytycznej do prognozowania krytycznej temperatury przepływu w zmiennych warunkach eksploatacyjnych za pomocą algorytmu Light Gradient Boosting Machine (LightGBM). Na tej podstawie opracowano odpowiedni wskaźnik bezpieczeństwa. Następnie, z wykorzystaniem sprzężonego modelu przepływu w sieci rurociągowej, wyznaczono krytyczną temperaturę na wlocie. Zaproponowano nowe kryterium oceny bezpieczeństwa oparte na „prawdopodobieństwie awarii i dotkliwości jej skutków". Metoda ta pozwala na precyzyjną ocenę poziomu bezpieczeństwa przepływu w rurociągach do transportu ropy naftowej. Zastosowane podejście wspiera bezpieczną eksploatację sieci rurociągowych na polach naftowych, a jednocześnie pozwala ograniczyć zużycie energii i poprawić efektywność ekonomiczną. Wyniki pokazują, że proponowany model umożliwia prognozowanie krytycznej temperatury przepływu ropy naftowej ze średnim błędem 6,4%, co potwierdza jego wysoką dokładność. Metodę oceny można stosować w zmiennych warunkach eksploatacyjnych. Jej zastosowanie w sieci rurociągowej umożliwiło opracowanie dynamicznego programu podgrzewania obejmującego cały cykl eksploatacyjny, co pozwoliło zmniejszyć zużycie gazu ziemnego o 57,7%.

Słowa kluczowe: przepływ ropy naftowej, sieć rurociągów przesyłowych na polu naftowym, ocena bezpieczeństwa procesu przepływu, strategia eksploatacji.

Corresponding authors: Zhang Z.Q., *1448072173@qq.com*; Zhang H.X., *zhxswpi@163.com*; He T.J., *363272635@qq.com*

Article contributed to the Editor: 06.05.2026. Approved for publication: 27.08.2026.

Introduction

The oilfield transmission pipeline network is a core component of surface engineering. It is responsible for transporting oil and gas from well pads and gathering stations to processing plants and export terminals. However, the conveyed media are highly complex. They are dominated by high-water-cut and high-pour-point crude oil. Fluid properties vary widely across different streams. Operating conditions fluctuate significantly. In cold regions, the situation becomes more severe. When the fluid temperature drops below the wall adhesion temperature, the adhesive force between waxy crude and the pipe wall exceeds the internal flow shear force. Wall adhesion is thus intensified rapidly. Once the temperature falls below the critical flow temperature of crude oil, flow assurance is compromised. Wax deposition and blockage are likely to occur (Heddouche, 2021; Mydlarz-Gabryk et al., 2014).

At present, wax deposition risk and the critical inlet temperature of pipelines transporting high-water-cut and high-pour-point crude oil remain difficult to quantify. To ensure stable transport, excessive heating is applied. This forces continuous high-load furnace operations, causing substantial energy waste (Gupta et al., 2015). In late-stage oilfield development, shifting operating conditions, such as water cut, alter crude oil flow characteristics (Andrade and Negrão, 2025; Yin et al., 2024). Consequently, initial heating schemes cannot accommodate these dynamic changes. Therefore, a predictive model for the critical flow temperature of crude oil across arbitrary compositions is urgently required. Additionally, wax deposition risk must be quantitatively identified to replace qualitative empirical estimations. This enables a dynamic temperature control strategy throughout the operational life cycle. This supports dynamic temperature control, improves energy efficiency, and maintains flow safety in oilfield pipeline networks.

Complex multiphase flow characterizes water-bearing crude oil in pipelines. The associated wax deposition risk is controlled by strongly coupled flow and heat transfer processes. Li et al. (2024) identified phase-change heat transfer and non-Newtonian rheology as core blockage mechanisms. Zhang et al. (2012) found significant deviations from existing models regarding flow patterns and pressure gradients in high-viscosity crude oil. Under gathering conditions, Yang et al. (2022) and Lin et al. (2022) confirmed the dominant impacts of liquid production, water cut, and ambient temperature on transport characteristics using visual experiments and alpine field data, respectively. Computationally, Sunday et al. (2023) built a 3D non-isothermal multiphase flow model to simulate inclination and flow velocity effects on cross-sectional distribution and heat exchange. Liu et al. (2024) and Rao et al. (2022) coupled fluid mechanics with aggregation kinetics. Building upon this, Sun et al. (2024) employed the population balance model (PBM) to simulate the hydraulic suspension systems of gelled crude oil. Their work revealed the modulating effects of flow velocity and water cut on the dispersed-phase particle size distribution and pressure drop, thereby elucidating the flow mechanisms within complex multiphase systems. In the realm of deposition prediction, Yu et al. (2021) revealed time-varying deposition accumulation under bubbly flow. Targeting static storage and transportation nodes, Wang et al. (2023) combined static settling experiments with molecular simulations to elucidate the flocculation and deposition evolution of heavy components (wax and asphaltenes) within storage tanks. Furthermore, Xu et al. (2021) used field experiments to clarify stratification and sudden pressure spikes induced by insufficient thermal mixing. However, existing studies mostly focus on single constant-diameter pipelines (Heddouche, 2021; Mydlarz-Gabryk et al., 2014; Zhao et al., 2018; Zou et al., 2023). System-level risk evaluations for the complex oilfield transmission pipeline network remain severely lacking.

Critical flow parameters of crude oil, such as wax appearance temperature (WAT) and pour point, dictate pipeline regulation. Traditionally, Fan et al. (2021), and Edris Joonaki et al. (2020) coupled cold finger experiments with equations of state to model molecular-level diffusion coefficients and asphaltene aggregation. However, solving thermodynamic equations becomes exceedingly cumbersome under arbitrary composition fluctuations within the oilfield transmission pipeline network. Fadi Alnaimat et al. (2020) identified artificial intelligence as essential for optimizing deposition prediction. Kouhi et al. (2025) utilized a least-squares support vector machine (LSSVM) model with density and pour point features to rapidly and accurately predict the WAT of arbitrary-composition crude oil. Shao et al. (2024) proposed a hybrid model based on seasonal-trend decomposition using locally estimated scatterplot smoothing (STL), eXtreme Gradient Boosting (XGBoost), and neural basis expansion analysis with exogenous variables (N-BEATSx) for load forecasting. Additionally, Nait Amar et al. (2022) applied a multilayer perceptron (MLP) neural network to quantitatively predict the deposited mass fraction. Therefore, machine learning provides a potential tool for rapid prediction and life-cycle evaluation in oilfield pipeline networks.

Practically, the microscopic mechanical interplay between gelled oil and the pipe wall dictates macroscopic flow boundaries. Hei et al. (2023) proposed the “wall-sticking temperature” as a more universal safety boundary for high-water-cut oilfields. In probing microscopic mechanisms, molecular dynamics (MD) and interfacial physical chemistry have provided foundational support. Li et al. (2023) elucidated the dominant role of van der Waals forces in the three-layer adsorption of wax molecules via MD simulations. Similarly, Lyu et al. (2022b) integrated molecular simulations with empirical experiments to uncover the microscopic mechanisms by which asphaltenes promote adhesion within unheated heavy oil systems. These findings corroborate the earlier interfacial theoretical conclusions of Zhang et al. (2020), and Li et al. (2022), which emphasized the prevailing influence of microscopic van der Waals forces in adhesion. Furthermore, Nguyen et al. (2023) leveraged surface energy and extended Derjaguin-Landau-Verwey-Overbeek (XDLVO) theory to analyze the effects of polar forces and interfacial interactions on the aggregation and deposition of asphaltene particles. Concurrently, Zhou et al. (2022) and Huang et al. (2019) quantified temperature and asphaltene effects on contact angles and adhesion forces using triaxial devices and atomic force microscopy (AFM), respectively. For macroscopic boundary prediction, Lyu et al. (2022a) formulated an adhesion energy model under shear flow conditions. Grounded in experimental data and Derjaguin-Landau-Verwey-Overbeek (DLVO) theory (which quantifies van der Waals and electrical double-layer forces), this model successfully determined the minimum safe gathering temperature for crude oil. Targeting ultra-high water cut (>90%) scenarios, Qin et al. (2025) dissected the critical role of yield stress in oil-water two-phase flow and adhesion, subsequently developing low-temperature gathering prediction software demonstrating exceptional field accuracy (error ≤2°C). Additionally, Qin et al. (2025) applied XDLVO theory to reveal the three-state ”slip-stick-adhesion” evolution of crude oil post-shutdown, establishing a safe temperature prediction model via force balance. Furthermore, Zhou et al. (2025) determined wall-sticking temperature limits for unheated gathering during high-water-cut periods via field tests. Regarding anti-adhesion regulation, Zhu et al. (2018) dispersed and activated asphaltenes by optimizing heat treatment temperatures. Li et al. (2020) developed underwater superoleophobic surface coatings to suppress wall adhesion. The aforementioned studies confirm that the adhesion critical point, defined based on mechanics, more accurately reflects the actual physical flow state than the traditional wax phase onset temperature.

In complex multiphase systems, quantitative relationships between compositions and the critical flow temperature of crude oil remain unclear. Additionally, evaluation frameworks for wax deposition risk within the oilfield transmission pipeline network are absent. Consequently, constant-heating modes fail to balance safety and energy conservation. Therefore, this study addresses three key questions: how to predict the critical flow temperature under variable operating conditions, how to determine the critical inlet temperature of pipelines, and how to establish a quantitative flow safety assessment framework for dynamic heating control. To address these questions, dynamic critical-temperature tests were conducted to obtain safety indicators that reflect actual flow behavior. Subsequently, a LightGBM algorithm was employed to construct a predictive model for the critical flow temperature of crude oil under arbitrary conditions. The predicted critical flow temperature was then coupled with multiphase flow calculations to estimate the critical inlet temperature of the pipeline. Finally, a two-dimensional failure probability-consequence severity criterion was established to classify the flow safety status of the oilfield transmission pipeline network. This framework supports the determination of inlet heating temperatures and the formulation of dynamic heating-control schemes. It also provides a practical basis for improving flow safety, reducing energy consumption, and supporting oilfield integrity management.

The primary innovations and contributions are as follows:

1. Unlike traditional wax appearance temperature (WAT)-based strategies, this study uses the critical flow temperature determined from dynamic wall-adhesion behavior as the safety boundary. This boundary better reflects the actual transition from stable flow to deposition-induced blockage in high-water-cut and high-pour-point crude oil.
2. Compared with previous adhesion-temperature studies that mainly measured wall-sticking temperatures under specific experimental or field conditions, this study establishes a data-driven prediction model. The model can estimate the critical flow temperature under different water cuts, pour points, and flow velocities. Therefore, it can support dynamic thermal control under variable operating conditions.
3. Compared with existing machine-learning studies that mainly focus on wax appearance temperature, wax deposition amount, or single-pipeline prediction, this study couples the LightGBM prediction model with multiphase flow calculations. This coupling enables the critical inlet temperature to be determined for an oilfield pipeline network rather than for an isolated pipe section.
4. A quantitative flow safety assessment framework based on failure probability and consequence severity is proposed. This framework links critical temperature prediction, hydraulic-thermal simulation, risk classification, and tiered heating control. It provides a practical basis for reducing energy consumption while maintaining flow assurance in oilfield pipeline networks.

Establishment of the flow-process safety quantitative evaluation method

The technical route for dynamically assessing and controlling wax deposition risk in the oilfield transmission pipeline network is shown in Figure 1. Initially, field-sampled crude oil

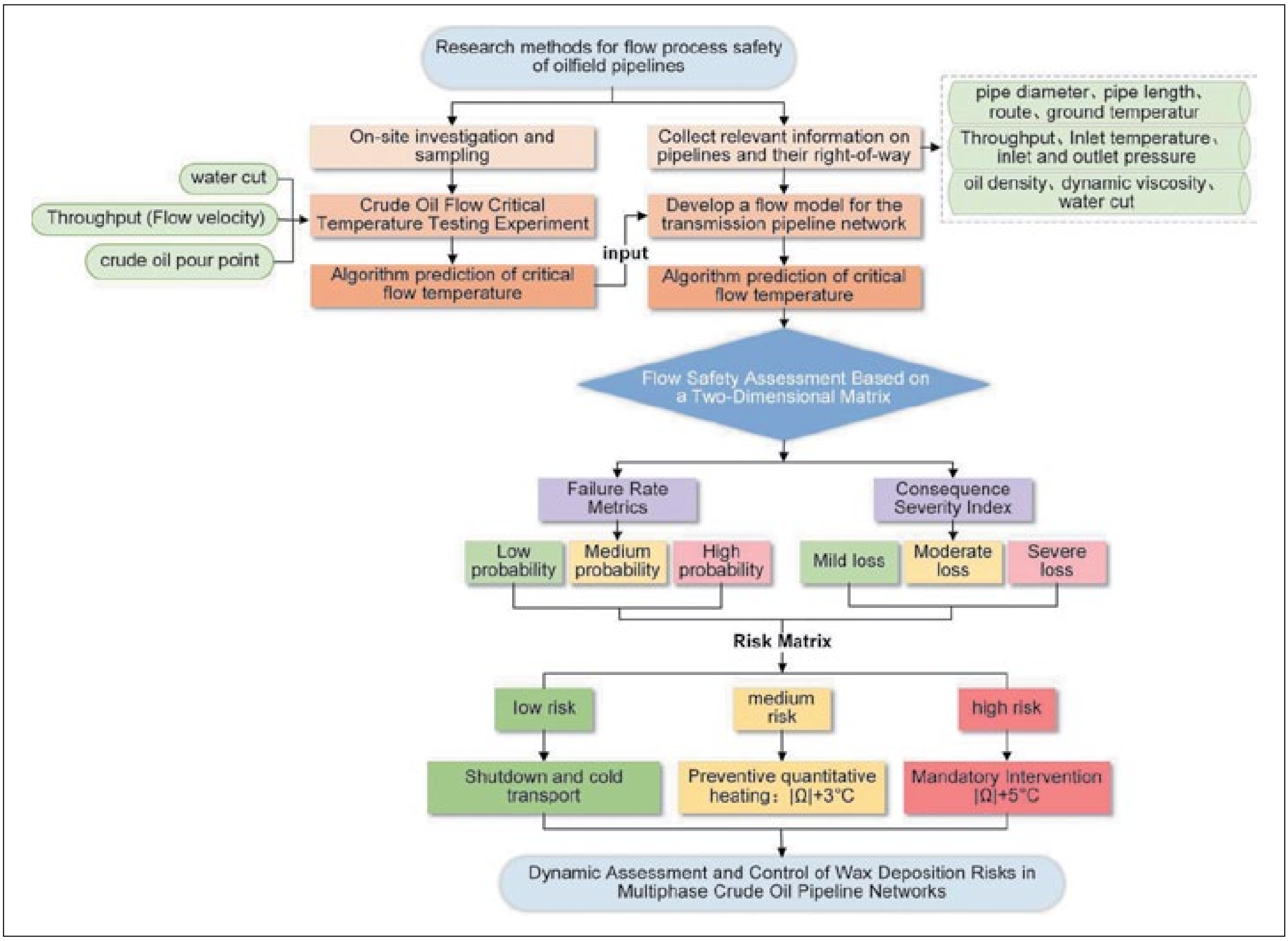

Figure 1. Technical route for dynamic assessment and control of wax deposition risk in oilfield pipeline networks

underwent critical flow temperature experiments. Concurrently, fluid properties, environmental data, and operational parameters were utilized to establish a flow model, calculating network-wide temperatures and pressures. Subsequently, the experimental datasets trained a LightGBM algorithm to predict the critical flow temperature of crude oil under arbitrary conditions. These predictions were combined with a multiphase flow calculation model to determine the critical inlet temperatures for the pipelines. Ultimately, evaluating these inlet temperatures, incoming fluid temperatures, and consequence severities established the dynamic risk control method. This method supports life-cycle heating optimization while maintaining flow safety and reducing energy consumption.

Determination of the Critical Flow Temperature of Crude Oil

To determine true flow boundaries, the traditional thermodynamic wax appearance temperature (WAT) was discarded. Instead, the critical flow temperature of crude oil was redefined by the adhesion force between gelled oil and the pipe wall. Mechanistically, initial fine wax crystals are dispersed by fluid shear, permitting macroscopic flow. However, as cooling progresses, wall adhesion exceeds fluid shear, rapidly triggering macroscopic solid deposition (wall-sticking). This reduces the effective flow cross-section and increases friction, thereby increasing wax deposition risk. Therefore, the adhesion-based boundary is more directly related to the observed transition from stable flow to wall adhesion.

Experimentally, crude oil sampled from the oilfield transmission pipeline network was dehydrated and emulsified. The critical flow temperature of crude oil was then measured via dynamic wall-sticking simulations. Finally, these empirical datasets trained a LightGBM algorithm to predict this critical temperature under arbitrary operating conditions.

Experimental Measurement of the Critical Flow Temperature of Crude Oil

By simulating realistic field pipeline conditions, this experiment investigated the flow and microscopic wall-adhesion behaviors of crude oil across varying water cuts during the cooling process, accurately capturing the wall-adhesion temperatures under specific conditions. Authentic field pipe material (fiberglass) was utilized as the deposition substrate. Coupled with water-bath cooling and magnetic shearing, a dynamic testing environment was constructed to simulate the actual flow history of the pipeline network. Ultimately, the critical flow temperature of crude oil was determined by quantitatively identifying the mass inflection point of the wall-adhered crude oil across diverse temperature gradients.

1. Experimental materials:
   Field-sampled crude oil was utilized. To eliminate thermal and shear histories and ensure property uniformity, electrical and distillation dehydration were performed using an APT-8 dehydrator. Subsequently, uniform preheating yielded the base oil for formulating emulsions with varying water cuts.
2. Experimental equipment:
   The experimental equipment included an APT-8 dehydrator, a DF-101S thermostatic magnetic stirrer, and a self-made device for measuring the critical flow temperature, as shown in Fig. 2. To replicate actual pipeline environments, a field-salvaged fiberglass pipe section served as the immersion element. A 6-HJ-5 digital stirrer was used to regulate the equivalent flow velocity of crude oil, while a thermostatic water bath with an external probe provided accurate temperature control.
3. Experimental procedure:
   3.1. Emulsions of crude oil with varying water cuts were formulated via one-step water addition and stirred (70°C, 1300 r/min, 15 min). To ensure reproducibility, identical-condition emulsions were batch-prepared and frozen at –2°C prior to use.
   3.2. The mass of the blank glass-fiber-reinforced plastic (GFRP) sample was weighed.
   3.3. 200 mL of crude oil emulsion was added to the beaker, the GFRP sample was placed inside, the magnetic stirring system was activated, the temperature-controlled water bath was set to the predetermined temperature, stirring was performed at a specific speed, and ice water was added to the beaker for cooling at a rate of 0.5°C/min.
   3.4. When the temperature of the emulsion reached the target value, stirring was continued for 10 minutes under constant temperature conditions.
   3.5. After soaking, the GFRP sample with oil residue adhering to its surface was removed using tweezers. It was then tilted at a 45° angle until no oil dripped before weighing. The difference in mass between this GFRP sample and the blank GFRP sample was calculated.
   3.6. The above steps were repeated until a sudden change in adhesion mass was observed. The temperature at which this occurred was identified as the critical flow temperature of the crude oil under the given condition. Crude oil adhesion reduces the flow area of pipelines, leading to increased pressure drop. Therefore, field pressure drop data should be collected to validate the experimental results, ensuring the accuracy and validity of the experiment.

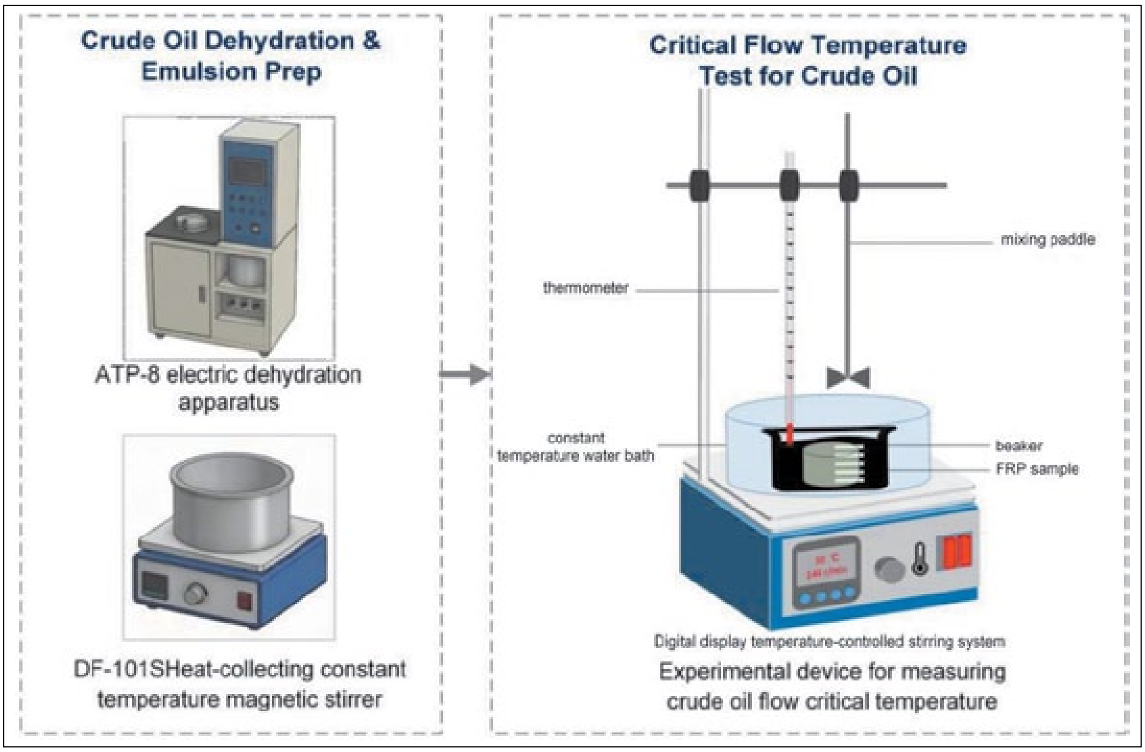

Figure 2. Experimental equipment for measuring the critical flow temperature of crude oil under simulated cooling and flowing conditions

Crude Oil Flow Critical Temperature Prediction

To predict the critical flow temperature of crude oil under variable field conditions, predictive modeling was conducted using the experimental results. To evaluate the suitability of different machine-learning algorithms for critical flow temperature prediction, LightGBM, XGBoost, support vector regression (SVR), and back-propagation neural networks (BPNNs) were established using the same experimental dataset and the same training-test split. These models were evaluated using mean squared error (MSE), root mean squared error (RMSE), mean absolute error (MAE), mean absolute percentage error (MAPE), and the coefficient of determination (R^2). The comparison results are presented in Section *Prediction of Crude Oil Flow Critical Temperature Using LightGBM Algorithm*. Based on the overall prediction performance and the ability to provide feature-importance interpretation, LightGBM was selected as the main model for subsequent analysis. A total of 100 experimental samples were used to develop the model. The input variables included water cut, crude oil pour point, and flow velocity, while the output variable was the critical flow temperature of crude oil. The samples covered crude oils collected from different transfer stations, with water cuts of 55%, 65%, and 70% and equivalent flow velocities of 0.90, 1.36, and 1.81 m/s. To ensure that both the training and test datasets represented different crude oil sources and operating conditions, the dataset was randomly divided into a training set and a test set at a ratio of 80:20.

The main hyperparameters of the LightGBM model were selected based on preliminary trials, prediction performance, and overfitting-control considerations. These parameters included the number of trees, learning rate, maximum tree depth, number of leaves, minimum samples per leaf, and regularization coefficients. To reduce overfitting under the limited sample size, tree depth and leaf number were constrained, and regularization terms were introduced during model training. Model performance on the training and test sets was then compared using MSE, RMSE, MAE, MAPE, and R^2 to evaluate the generalization ability of the model.

Within the gradient boosting framework, Gradient-based One-Side Sampling (GOSS) was used to improve data-sampling efficiency. A leaf-wise tree growth strategy with depth limitation was adopted to improve prediction accuracy while controlling model complexity. Classification and Regression Trees (CARTs) were iteratively trained through a forward additive process to capture the nonlinear relationship among water cut, pour point, flow velocity, and critical flow temperature. The feature importance of each input variable was then extracted from the trained LightGBM model to support interpretation of variable influence. The computational workflow of the algorithm is shown in Figure 3.

To prevent overfitting, the loss function is expanded using a second-order Taylor series, with a regularization term added to reduce model variance. The loss function is expressed as:

$$Obj(x)=\sum_{i=1}^{n} l(y_i,\hat{y}_i)+\sum_{k}^{j=1}\Omega(f_j), f_j \in f \quad (1)$$

where $l(y_i,\hat{y}_i)$ denotes the training error of sample x_i, $\Omega(f_j)$ denotes the regularization term of the j-th tree.

The optimized function after second-order Taylor series expansion and the Gain function are respectively

$$Obj(x)=-\frac{1}{2}\sum_{T}^{j=1}\frac{G_j^2}{H_j+\lambda}+\gamma T \quad (2)$$

$$Gain=\frac{1}{2}\left[\frac{G_L^2}{H_L+\lambda}+\frac{G_R^2}{H_R+\lambda}-\frac{(G_L+G_R)^2}{H_R+H_L+\lambda}\right]-\gamma \quad (3)$$

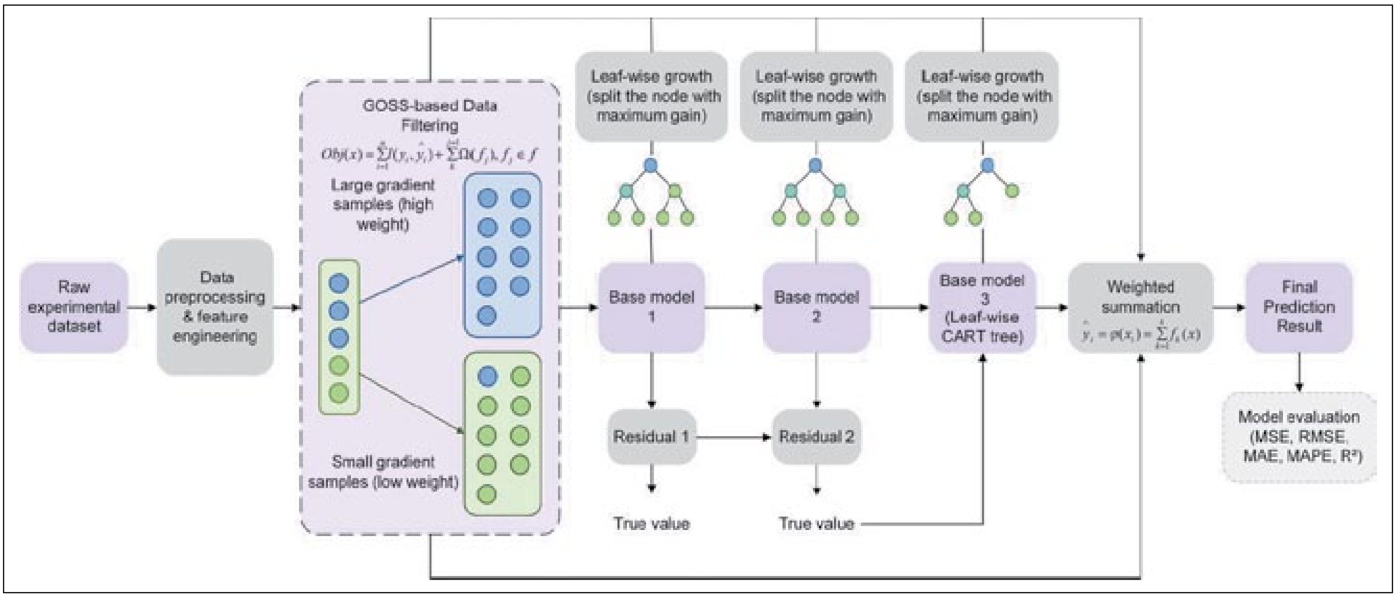

Figure 3. Basic computational workflow of the LightGBM model for predicting the critical flow temperature of crude oil

where $Gain$ denotes the loss of the objective function after tree splitting; G_j denotes the sum of the first derivatives of the loss function; H_j denotes the sum of the second derivatives of the loss function; γT denotes the penalty term; G_L, G_R denote the sums of the first derivatives of the left and right loss functions; H_L, H_R denote the sums of the second derivatives of the left and right loss functions; λ denotes the penalty coefficient.

The general formula for the prediction results of the tree model is:

$$\hat{y}_i = \varphi(x_i) = \sum_{k=1}^{k} f_k(x), f_k \in F \tag{4}$$

where $\hat{y}_i$ denotes the prediction result; $\varphi(x_i)$ denotes the prediction score of Sample x_i; k denotes the total number of trees; f_k denotes the k-th decision tree; F denotes the function space corresponding to the decision tree.

Conventional Gradient Boosting Decision Tree (GBDT) models incur substantial computational overhead when processing massive datasets. To address this, the LightGBM algorithm employed in this study incorporates the GOSS (Gradient-based One-Side Sampling) mechanism and histogram-based algorithms. The split variance gain formula for GOSS is expressed as:

$$V_j(d) = \frac{1}{n}\left[\frac{\left(\sum_{x_i \in A_l} g_i + \frac{1-a}{b}\sum_{x_i \in B_l} g_i\right)^2}{n_l^i(d)} + \frac{\left(\sum_{x_i \in A_r} g_i + \frac{1-a}{b}\sum_{x_i \in B_r} g_i\right)^2}{n_r^i(d)}\right] \tag{5}$$

where n denotes the total number of instances; g_i denotes the absolute value of the gradient for the i-th instance; A_l and A_r denote the subsets of large-gradient instances partitioned into the left and right child nodes, respectively; B_l and B_r denote the subsets of sampled small--gradient instances partitioned into the left and right child nodes, respectively; a denotes the retention ratio of large-gradient instances; b denotes the sampling ratio of small-gradient instances; and $n_l^i(d)$, $n_r^i(d)$ denote the total number of instances in the left and right child nodes at the split point d, respectively.

The equation for histogram subtraction is expressed as:

$$H_{parent} = H_{left} + H_{right} \tag{6}$$

where H denotes the histogram of discretized features at the corresponding node (comprising the first- and second--order gradient statistics).

To evaluate the predictive performance of the model, metrics such as Mean Squared Error (MSE), Root Mean Squared Error (RMSE), and the correlation coefficient (R^2) are selected as measures of model quality. Lower values of MSE and RMSE indicate smaller prediction errors generated by the model.

$$MSE = \frac{1}{n}\sum_{n}^{i=1}(y_i - \hat{y}_i)^2 \tag{7}$$

$$RMSE = \sqrt{\frac{1}{n}\sum_{n}^{i=1}\left(\hat{y}_i - y_i\right)^2} \tag{8}$$

$$R^2 = 1 - \frac{\sum_{n}^{i=0}\left(y_i - \hat{y}_i\right)^2}{\sum_{n}^{i=0}\left(y_i - \hat{y}_i\right)^2} \tag{9}$$

where n is the total number of data points; y_i is the i-th actual value; $\hat{y}_i$ is the i-th predicted value.

Establishing a Determination Method for the Critical Inlet Temperature via Multiphase Flow Calculations

To maintain flow safety during the transport of high-water-cut, high-pour-point crude oil, the terminal pipeline temperature T_2 must strictly exceed the critical flow temperature of crude oil. Using this as the strict boundary condition, multiphase flow theory back-calculates the critical inlet temperature of the pipeline T_1. Comparing T_1 with the actual inlet temperature identifies wax deposition risk and guides dynamic thermal optimization. Thus, T_1 serves as a key early-warning indicator for pipeline flow safety. Methodologically, an oil-water two-phase flow model encompassing mass, momentum, and energy conservation was established (Pham et al., 2017; Li, 2010). Simulations were executed by inputting pipeline, fluid, and environmental parameters, anchored by the predicted critical flow temperature of crude oil as the terminal boundary T_2. Subsequently, field operational data (temperature and pressure) validated the model, enabling the precise derivation of T_1 for individual pipelines.

1. Mass Transportation Equations

For a mass field denoted m_i traveling at velocity U_i the mass transport equation is:

$$\partial_t m_i + \partial_z(m_i U_i) = \sum_j \Psi_{ji} + G_i \tag{10}$$

where ∂_t denotes differentiation in time, ∂_z denotes spatial differentiation, Ψ_{ji} denotes the rate of mass transfer between the j-th and i-th mass field, that is, dispersions, droplet deposition and entrainment, and phase transitions, and G_i denotes any mass source/sink.

- Mass transportation equation for oil in liquid layers:

$$\partial_t m_{Hl} + \partial_z(m_{Hl} U_{Hl}) = \Psi_{Hl} + G_{Hl} \tag{11}$$

- Mass transportation for water in liquid layer:

$$\partial_t m_{Wl} + \partial_z (m_{Wl} U_{Wl}) = \Psi_{Wl} + G_{Wl} \tag{12}$$

where subscripts H, W, l denote oil phase, water phase and liquid layer, respectively.

2. Momentum Balance Equations

For a momentum field denoted $m_i U_i$ the momentum balance equation is:

$$\begin{aligned}&\partial_t (m_i U_i) + \partial_z (m_i U_i^2) = \\ &= m_i \cdot g \cdot \cos(\varphi) + P_i + G_i U_i + \Sigma_j (\Psi_{ji}^+ U_j - \Psi_{ji}^- U_i) + \\ &+ \Sigma_j F_{ji}' (U_j - U_i) - F_i^w U_i\end{aligned} \tag{13}$$

where ∂_t denotes differentiation in time, ∂_z denotes spatial differentiation, g is the acceleration of gravity, φ is the pipe angle relative to the gravitational vector, P_i is the pressure force, $G_i U_i$ is the momentum contribution corresponding to the mass source/sink G_i, F'_{ji} are friction forces between the i-th and j-th mass field, and F^w denotes the wall friction. Ψ_{ji} denotes momentum contributions corresponding to the mass transfer between the j-th and i-th mass field. In the equation above $\Psi^+{}_{ji}$ accounts for a net contribution from mass field i to j while $\Psi^-{}_{ji}$ accounts for a net contribution from mass field j to i.

3. Conservation of Volume

Given the pressure, P, and the volume fractions, α_i, the mass transport equations and momentum balance equations above can be used to determine the masses, m_i, and velocities, U_i. Using the trivial constraint that the volume of the fluid equals to the volume of the pipe it resides in together with the equation of state, the volume equation is given by:

$$\begin{aligned}&\Sigma_L \left(\frac{m_L}{\rho_L^2}\frac{d\rho_L}{dP}\right)\partial_t P + \\ &+ \Sigma_L \left(\frac{m_L}{\rho_L^2}\frac{d\rho_L}{dT}\right)\partial_t T + \Sigma_L \frac{1}{\rho_L}(\partial_z (m_L U_L) + G_L) = 0\end{aligned} \tag{14}$$

where L denotes the existing phases.

4. Energy Balance

The energy balance equation for a mass field m_i can be written as:

$$\partial_t (m_i E_i) + \partial_z (m_i U_i H_i) = S_i + Q_i + \Sigma_j T_{ij} E_j \tag{15}$$

where E_i denotes the field energy, H_i denotes the field enthalpy, S denotes enthalpy source/sink, Q is the heat flux through the pipe wall, and T_{ij} models the energy transfer between fields.

Safety Assessment and Integrity Management of Crude Oil Flow Technology

Initially, the most frequent monthly operational conditions within the oilfield transmission pipeline network were aggregated. Under these conditions, the LightGBM algorithm predicted the critical flow temperature of crude oil, while a multiphase flow model computed the critical inlet temperature of the pipeline. Per the GB/T 50253–2014 standard, heated transport strictly requires local temperatures to exceed the pour point of crude oil by 3–5°C across the entire route. Based on these thermal boundaries, a two-dimensional failure probability-consequence severity matrix was proposed as the flow safety evaluation criterion:

1. Failure Probability Index (P)

The thermal failure index, Ω, is defined as:

$$\Omega = T - T_1 \tag{16}$$

where T denotes the actual incoming fluid temperature of the pipeline; T_1 denotes the critical inlet temperature.

This index strictly dictates the clogging probability:

$$P = \begin{cases} P_1, \Omega > 3°C \\ P_2, 0°C < \Omega \le 3°C \\ P_3, \Omega \le 0°C \end{cases} \tag{17}$$

where P denotes the failure probability index; P_1 denotes a low failure probability, indicating thermal sufficiency; P_2 denotes a medium failure probability, representing a critical boundary state; and P_3 denotes a high failure probability, signifying severe thermal inadequacy.

2. Consequence Severity Index (S)

Blockages in pipelines transporting crude oil primarily inflict economic losses via system shutdowns. To transcend absolute throughput limitations and enhance model universality across diverse topologies within the oilfield transmission pipeline network, a relative throughput loss coefficient α is introduced:

$$\alpha = \frac{Q_i}{Q_{total}} \tag{18}$$

where Q_i denotes the daily throughput of the failed pipeline; and Q_{total} denotes the total daily throughput of the pipeline network.

Coupling α with the pipeline's hierarchical function dictates the severity rating:

$$S = \begin{cases} S_1, \alpha \le 30\% \text{ or Peripheral branch lines} \\ S_2, 30\% < \alpha \le 70\% \text{ or Regional gathering trunks} \\ S_3, \alpha > 70\% \text{ or Core export hubs} \end{cases} \tag{19}$$

where S denotes the consequence severity rating; S_1 denotes a mild loss, indicating localized impacts; S_2 denotes a moderate loss, representing intermediate impacts; and S_3 denotes a severe loss, signifying catastrophic impacts.

3. Risk Matrix and Quantitative Thermal Control Strategies

By coupling the above failure probability index and consequence severity index, a 3×3 flow safety risk assessment matrix was established as shown in Table 1. The flow state of the pipeline network was classified into three comprehensive risk levels: low, medium and high. Based on this, a stepped and quantitative dynamic thermal temperature control strategy was formulated, as presented in Table 2: Low Risk: Denotes a stable thermal state for crude oil. Unheated gathering or cold transport is universally executed to maximize energy conservation without compromising safety. Medium Risk: Indicates a thermal boundary state or localized throughput limitations. "Preventive quantitative heating" is deployed, precisely elevating the heater temperature by $|\Omega| + 3°C$ to ensure stable flow transitions while eliminating energy waste. High Risk: Indicates severe wax deposition risk, which may lead to system shutdowns. Mandatory intervention is triggered immediately, and heaters are operated at full load to increase the temperature by $|\Omega| + 5°C$, thereby maintaining flow safety in the pipeline network.

Table 1. Risk matrix

Probability	Consequence		
	S_1: Mild loss	S_2: Moderate loss	S_3: Severe loss
P_3: High probability	Medium	High	High
P_2: Medium probability	Low	Medium	High
P_1: Low probability	Low	Low	Medium

Table 2. Tiered thermal control strategy

Risk level	Measure
Low risk	Execute unheated cold transport
Medium risk	Execute preventive heating: initiate quantitative thermal compensation at $|\Omega| + 3°C$
High risk	Trigger mandatory intervention: apply full-load heating at $|\Omega| + 5°C$

Case Study

On-site Investigation and Sampling

Taking the annual operation of an oilfield transmission pipeline network – comprising three transfer stations (T_1, T_2, and T_3) and three pipelines (A, B, and C) – as a case study, where pipelines B and C are connected in parallel, the structural schematic is shown in Figure 4. The fundamental parameters of each pipeline, the physical properties of the transported oil products, and the operational parameter ranges are detailed in Table 3. All oil products are wax-containing crude oil with high pour points and water cuts ranging from 40% to 90%.

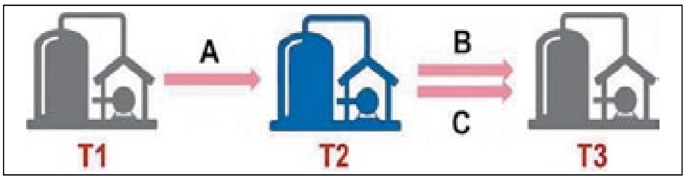

Figure 4. Schematic diagram of the oilfield pipelines

Table 3. Parameter range of the pipelines

Parameter type	Parameter item	T_1–T_2 pipeline A	T_2–T_3 pipeline B/C
Pipeline parameters	Pipe length [km]	14.2	22.4
	Pipe diameter [mm]	209	263.1
	Wall thickness [mm]	9.1	11.2
	Design pressure [MPa]	5.2	5.2
Crude oil properties	Density [kg/m^3]	830	825
	Viscosity at 50°C [mPa·s]	6.95	9.51
	Average wax content [%]	7.03	9.85
	Pour point [°C]	13.0	16.0
Operating parameters	Daily throughput [t]	2400~3600	1000~1600
	Water cut [%]	45%~65%	50%~70%
	Starting temperature [°C]	15~27	15~27
	Starting pressure [MPa]	1.43~2.71	2.23~3.01
	Ground temperature [°C]	3~11	

Dehydration of Crude Oil and Preparation of Emulsions

Electrical dehydration units were employed to remove water from crude oil at various transfer stations, producing crude oil emulsions with different water-content ratios. These emulsions were subsequently frozen for storage, as illustrated in Figure 5.

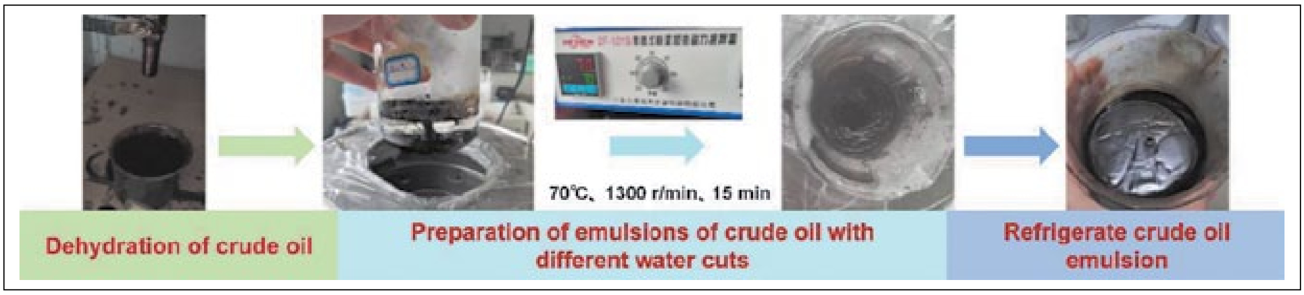

Figure 5. Crude oil dehydration and preparation of emulsions with different water cuts

Crude Oil Flow Critical Temperature Testing Experiment

As shown in Figure 6, under conditions of T_1 transfer station oil with 55% water cut and an experimental rotational speed of 433 r/min, the mass of the GFRP sample immersed for 10 minutes continued to increase as the crude oil temperature gradually decreased. It reached a peak at 14°C, then underwent a sudden mass change at 12°C, followed by a sharp rise in the GFRP sample's mass. This indicates a significant increase in the crude oil's sticky oil mass. Therefore, the wall adhesion temperature of T_1 oil under these operating conditions is determined to be 12°C. The pressure drop observed during the on-site cooling process aligns with the pattern of wall adhesion mass variation measured in the experiment.

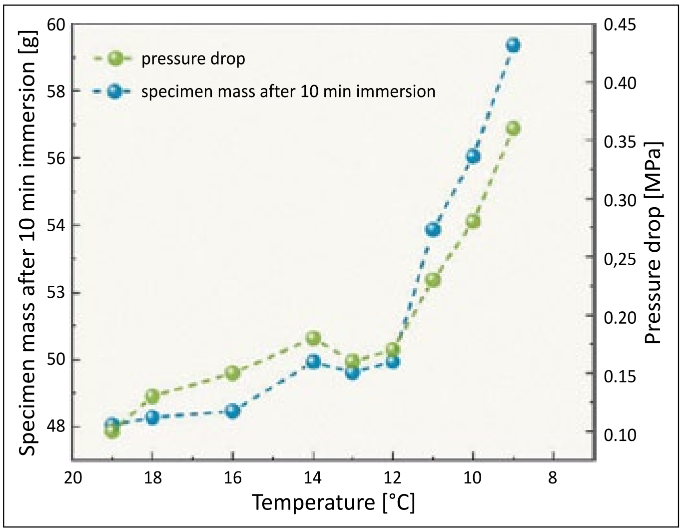

Figure 6. Experimental verification of the critical flow temperature of crude oil

Crude oil from different transfer stations (T_1, T_2, T_3) were used to prepare crude oil emulsions with varying water cuts (55%, 65%, 70%) and different rotational speeds (433 r/min, 650 r/min, 866 r/min). The experiment was repeated for a total of 100 sets, and the critical flow temperature of crude oil is shown in Figure 7 (Rotational speeds of 433 r/min, 650 r/min, and 866 r/min correspond to flow velocities of 0.9 m/s, 1.36 m/s, and 1.81 m/s, respectively). The results in Figure 7 show that the critical flow temperature varied under different crude oil sources, water cuts, and flow velocities. This indicates that the flow boundary of high-water-cut and high-pour-point crude oil is not a fixed temperature value. Instead, it is jointly controlled by crude oil properties and operating conditions.

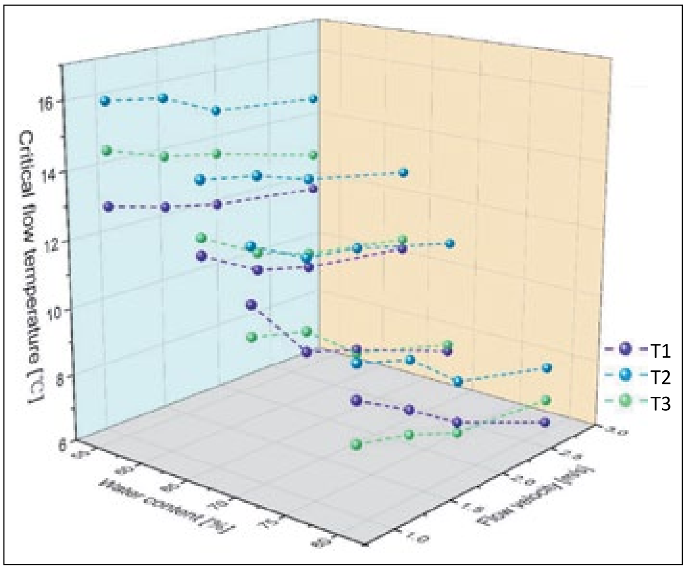

Figure 7. Experimental results of critical flow temperature for oilfield pipelines

Prediction of Crude Oil Flow Critical Temperature Using LightGBM Algorithm

The prediction performance of LightGBM, XGBoost, SVR, and BPNNs was compared using MSE, RMSE, MAE, MAPE, and R^2, as shown in Table 4. On the test set, LightGBM achieved an MSE of 0.272, an RMSE of 0.521, a MAPE of 3.708%, and an R^2 of 0.935. Compared with the other models, LightGBM showed the lowest MSE and RMSE and the highest R^2, indicating better overall generalization performance. Although its MAE was slightly higher than those of XGBoost and SVR, the difference was small. Therefore, LightGBM was selected as the main prediction model for critical flow temperature under variable operating conditions.

To provide a preliminary interpretation of the influence of input variables, the feature importance values obtained from the trained LightGBM model were normalized as follows:

Table 4. Performance comparison of different machine-learning models on the training and test sets

Model	Dataset	MSE	RMSE	MAE	MAPE%	R^2
LightGBM	Training set	0.117	0.343	0.279	2.817	0.983
	Test set	0.272	0.521	0.425	3.708	0.935
XGBoost	Training set	0.122	0.350	0.266	2.692	0.982
	Test set	0.274	0.524	0.413	3.729	0.934
SVR	Training set	0.235	0.485	0.284	2.986	0.966
	Test set	0.290	0.538	0.399	3.703	0.930
BPNNs	Training set	0.240	0.489	0.366	3.517	0.965
	Test set	0.371	0.609	0.479	4.274	0.911

$$S_i = \frac{FI_i}{\sum_{i=1}^{n} FI_i} \times 100\% \tag{20}$$

where FI_i denotes the feature importance of the i-th input variable, S_i denotes its normalized feature-importance value, and n denotes the total number of input variables. The calculated normalized feature-importance values are listed in Table 5.

The results show that water cut had the highest contribution, accounting for 65.00% of the total feature importance. Pour point contributed 24.10%, while flow velocity contributed 10.90%. Therefore, the relative influence ranking of the input variables was water cut > pour point > flow velocity. In physical terms, an increase in water cut can change the oil-water dispersion state and enhance the interaction among wax crystals, emulsified water droplets, and the pipe wall, making the critical flow temperature more sensitive to temperature variation. A higher pour point usually indicates poorer low-temperature flowability of crude oil, which tends to increase the critical flow temperature. Flow velocity affects the shear condition in the pipeline; an increase in flow velocity may weaken wall adhesion and deposition tendency to some extent, but its normalized feature-importance value in this dataset was lower than those of water cut and pour point. Therefore, the feature-importance results provide an interpretable indication of the relative influence of input variables, but they do not fully replace a formal sensitivity analysis based on controlled perturbations of input parameters. More systematic perturbation-based sensitivity analysis should be conducted in future work using a larger dataset.

The uncertainty of the prediction results was evaluated using the existing error indicators, including MSE, RMSE, MAE, MAPE, R^2, and the average relative error. As shown in Table 4, the LightGBM model achieved R^2 values of 0.983 and 0.935 for the training and test sets, respectively, indicating good fitting ability and generalization performance. For the test set, the MSE, RMSE, MAE, and MAPE were 0.272, 0.521, 0.425, and 3.708%, respectively. These results indicate that the model has acceptable prediction accuracy for engineering application. However, prediction uncertainty still exists. This uncertainty may be related to experimental measurement errors, emulsion preparation errors, differences in crude oil composition, conversion errors between stirring speed and equivalent flow velocity, and fluctuations in field operating conditions. Therefore, an appropriate safety margin should be considered when applying the predicted critical flow temperature to field thermal-control decisions.

Table 5. Normalized feature importance of input variables in the LightGBM model

Feature	Normalized feature importance
Water cut	65.00%
Pour point [°C]	24.10%
Flow velocity [m/s]	10.90%

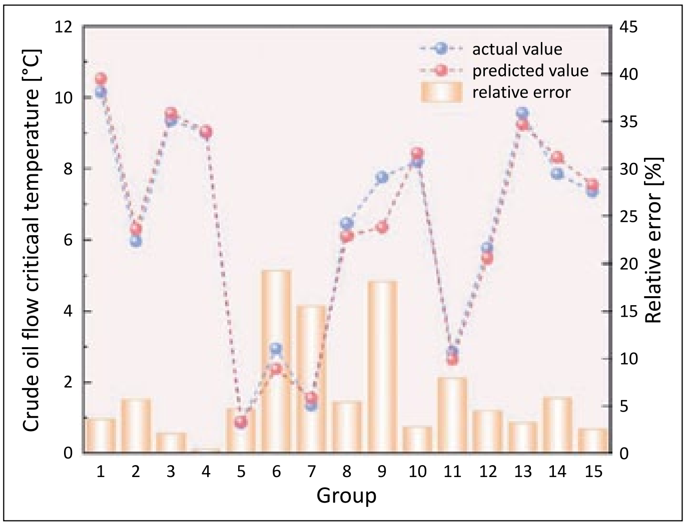

Figure 8. Prediction error analysis of critical flow temperature at oilfield transfer stations

Figure 8 shows the predicted and measured critical flow temperatures for crude oils from different transfer stations, together with the corresponding relative errors. The minimum, maximum, and average relative errors are 0.44%, 19.32%, and 6.4%, respectively. Most samples show relatively small deviations between predicted and measured values, whereas larger errors are observed only in a few cases. These larger deviations are mainly associated with operating conditions close to the transition from stable flow to wall adhesion, where small changes in emulsion state, crude oil composition, or equivalent flow velocity may lead to more obvious changes in the measured critical flow temperature. Therefore, the prediction results indicate that the LightGBM model can provide a useful temperature reference for subsequent critical inlet temperature calculation, but prediction uncertainty may increase near the flow-state transition boundary.

Flow model of transmission pipeline network

Incorporating crude oil properties, operational and pipeline parameters, and spatial routing conditions, a flow model for the oilfield transmission pipeline network was established.

Simulations were conducted on the flow parameters of the pipelines under operating conditions in February (the coldest month). Validation was performed using the outlet pressures from each field transfer station and the inlet temperatures at the terminal combined station, as shown in Figure 9. The relative errors were all within 3%, indicating a high degree of agreement between the model simulation results and the field data. This agreement suggests that the established multiphase flow model can describe the hydraulic and thermal behavior of the target pipeline network with acceptable accuracy. Therefore, the model can be used to calculate the critical inlet temperature under monthly operating conditions.

Figure 10 compares the monthly actual inlet temperatures with the calculated critical inlet temperatures. When the actual inlet temperature is higher than the critical inlet temperature,

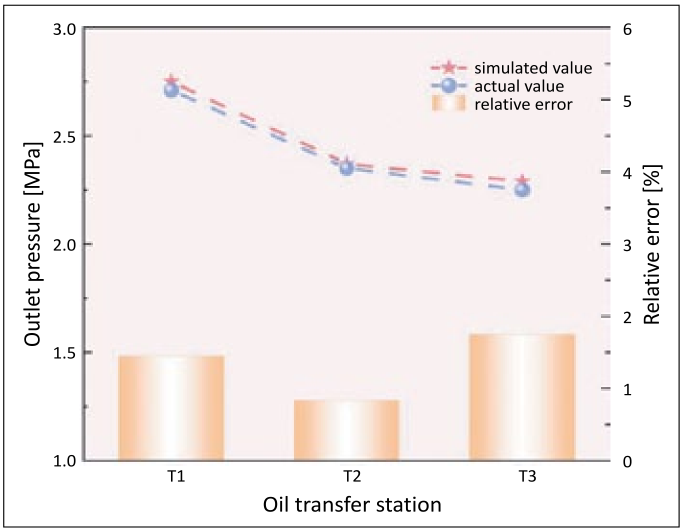

Figure 9. Flow model validation for the transmission pipeline network

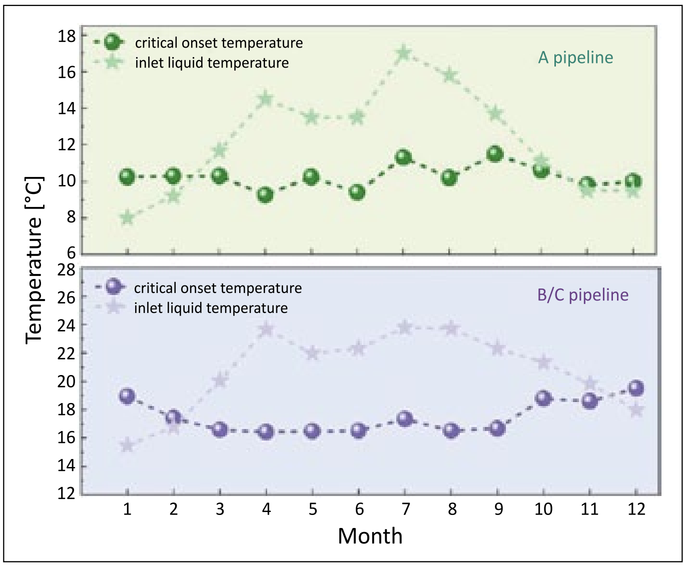

Figure 10. Comparison between monthly inlet temperature and critical inlet temperature of the transmission pipeline

the pipeline has a sufficient thermal margin and can maintain stable flow. In contrast, when the actual inlet temperature approaches or falls below the critical inlet temperature, the thermal margin becomes insufficient, and wax deposition risk increases. This comparison provides a direct basis for calculating the failure probability index and classifying the monthly flow safety state of each pipeline.

Safety Assessment of Flow-Process for Transmission Pipeline Network

Operational parameters of the target network from January to December were integrated into the risk matrix. For Pipeline A (the core trunk line), the consequence severity strictly remained at S_3. Conversely, the relative throughput loss coefficient α for branch lines B and C fluctuated dynamically between 23.7% and 43.3%, prompting autonomous severity rating transitions between S_1 and S_2. Figure 11 details the resultant comprehensive risks and corresponding thermal control strategies. The safety states of all pipelines exhibited distinct seasonal dynamics. Serving as the principal trunk line, Pipeline A is subject to stringent safety constraints. During January–March and September–December – the coldest periods of the year – the pipeline consistently operates within a high-risk zone, necessitating the strict execution of a mandatory thermal intervention with a target temperature increment of 5.30°C to 7.25°C. Preventive monitoring is only applicable during the medium-risk period from April through August. In contrast, functioning as branch pipelines, Pipelines B and C encounter high-risk conditions solely during the severely cold months of January–February, necessitating mandatory thermal intervention with target increments ranging from 5.61°C to 8.47°C. Conversely, in December, a contraction in instantaneous throughput shifts

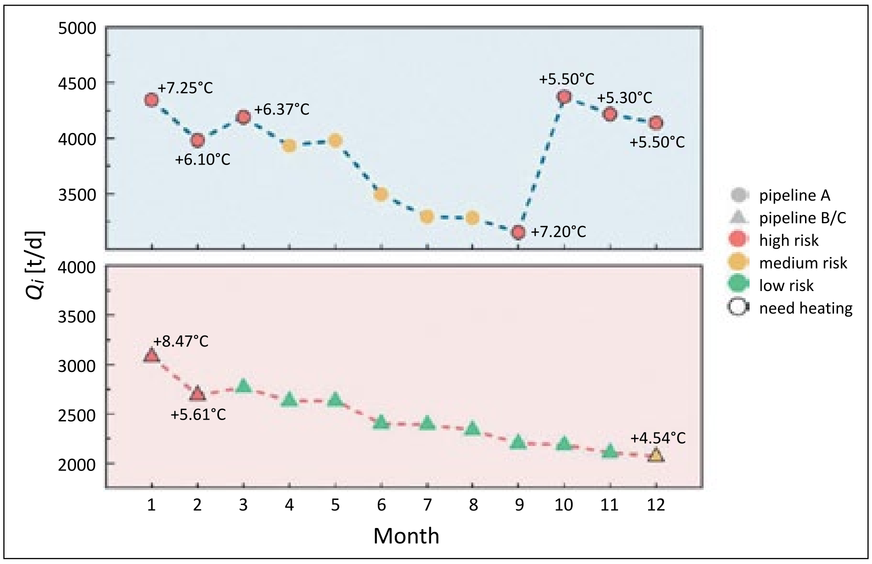

Figure 11. Monthly comprehensive risk levels and corresponding tiered thermal control strategies

their risk rating to medium, dictating preventive quantitative heating with a precise 4.54°C increment. During the remaining nine months, the branch lines were classified as low risk, indicating that unheated cold transport could be applied. These results show that the proposed risk matrix can convert monthly thermal margins and consequence severity into direct operational decisions. Therefore, Figure 11 provides the basis for implementing differentiated heating control among trunk and branch pipelines.

Economic Evaluation

To quantify the economic value of this safety evaluation model in field applications, a comparative energy consumption analysis was conducted between the dynamic thermal control and conventional operational strategies for the target network. Based on the thermal efficiency of field heaters, the required natural gas consumption (m³/d) was derived:

$$Gc\Delta T = qB_H\eta \tag{21}$$

where G denotes the mass flow velocity of the liquid phase (kg/d); c denotes the specific heat capacity of the liquid phase (kJ/(kg · °C)); $|\Omega|$ denotes the absolute value of the temperature difference between the incoming fluid temperature and the critical inlet temperature T_1 (°C); q denotes the daily natural gas consumption of the heater (m³/d); B_H denotes the combustion heating value of natural gas (39,800 kJ/m³); and η denotes the thermal efficiency of the heater (the field heater model is DH2500-Y/1.6/0.6-Q-18 with a thermal efficiency of 94%).

Benchmarking the proposed dynamic thermal control strategy against the actual heater operating times across the transfer stations, the original heating strategy recorded an annual natural gas consumption of 29,826.6 m³. Under the proposed strategy, natural gas consumption decreased to 12,623.7 m³, representing a 57.7% reduction. Assuming a natural gas price of 2.5 Chinese yuan (CNY)/m³, this optimization translates to an annual economic saving of 43,007.25 CNY. The comparison of annual natural gas expenditures between the original and proposed heating strategies is shown in Figure 12.

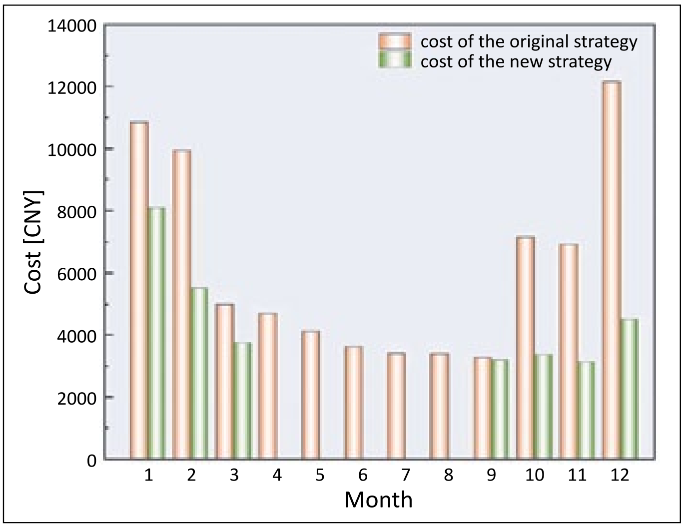

Figure 12. Comparison of annual natural gas expenditure between the proposed and original heating strategies

The economic analysis above provides an engineering estimate based on direct natural gas savings. However, the actual economic benefit may vary with seasonal ground temperature, short-term throughput changes, water-cut fluctuation, heater efficiency degradation, and natural gas price variation. These operational uncertainties may change the required heating intensity and, consequently, the final fuel-saving value.

In addition to direct energy savings, the proposed strategy may also reduce long-term maintenance costs. By avoiding unnecessary high-load heater operation during low-risk periods and applying quantitative heating only when required, the strategy can reduce heater operating time, thermal stress, equipment aging, and maintenance frequency. Therefore, the calculated saving should be interpreted as a conservative estimate under the current operating conditions, while the long-term economic benefit may be further improved when operational variability and maintenance effects are considered. The proposed strategy may be adapted to other oilfield pipeline networks after local calibration using site-specific crude oil properties, pipeline parameters, and operating data.

Conclusion

This study integrated experimental data with the LightGBM algorithm to establish a prediction model for the critical flow temperature under variable operating conditions. By coupling this parameter with the critical inlet temperature derived from multiphase flow calculations, a safety evaluation criterion based on a failure probability-consequence severity matrix was proposed to overcome the limitations of conventional single-threshold heating control. The application of this framework to a certain oilfield transmission pipeline network enabled the identification of flow safety states across hierarchical nodes and varying months, supporting a full-cycle, dynamic, and tiered thermal control strategy. The principal conclusions are summarized as follows:

1. The established model predicted the critical flow temperature of crude oil under different flow velocities and water cuts, with an average relative error of 6.4%.
2. A flow safety evaluation framework was developed to link critical temperature prediction, risk evaluation indices, tiered thresholds, and dynamic heating-control strategies.
3. Applying this framework to an oilfield transmission pipeline network revealed that Pipeline A (April–August) and Pipelines B/C (March–November) operated in secure flow states, permitting unheated cold transport. For the remaining months, target temperature increases for preventive quantitative heating were determined. Consequently, a full-cycle, dynamic operational scheme was formulated. Compared with the original heating strategy, the optimized approach reduced natural gas consumption by 57.7%, corresponding to an annual economic saving of 43,007.25 CNY.
4. The proposed method still has several limitations. The prediction model was developed using 100 experimental samples, and a larger dataset would further improve model robustness and reduce prediction uncertainty. In addition, the field validation was conducted using one oilfield transmission pipeline network, which may limit the generalizability of the framework. When the method is transferred to other pipeline networks, local calibration is required using site-specific crude oil properties, pipeline parameters, water-cut conditions, ground temperature, and operating data. Future work will focus on expanding the dataset and validating the proposed framework in more field cases.

Declaration of interest statement

The authors declare that they have no known competing financial interests or personal relationships that could have appeared to influence the work reported in this paper. Some or all data, models, or code that support the findings of this study are available from the corresponding author upon reasonable request.

Acknowledgment

This work is supported by the National Natural Science Foundation of China (52502432) and Natural Science Foundation of Sichuan Province (2025ZNSFSC1368).

References

Alnaimat F., Ziauddin M., Mathew B., 2020. Wax Deposition in Crude Oil Transport Lines and Wax Estimation Methods. *Intelligent System and Computing*, 191. DOI: 10.5772/intechopen.89459.

Amar M.N., Ghahfarokhi A.J., Ng C.S.W., 2022. Predicting wax deposition using robust machine learning techniques. *Petroleum*, 8(2): 167–173. DOI: 10.1016/j.petlm.2021.07.005.

Andrade D.E.V., Negrão C.O.R., 2025. Rheology of waxy oils: A critical review. *Applications in Engineering Science*, 21: 100202. DOI: 10.1016/j.apples.2024.100202.

Fan K., Li S., Li R., 2021. Development of wax molecular diffusivity correlation suitable for crude oil in wax deposition: Experiments with a cold-finger apparatus. *Journal of Petroleum Science and Engineering*, 205: 108851. DOI: 10.1016/j.petrol.2021.108851.

Gupta A., Anirbid S., 2015. Need of Flow Assurance for Crude Oil Pipelines: A Review. *International Journal of Computational Science & Engineering*, 6(2): 2015–2045.

Heddouche M., 2021. Modeling and Simulation of Multiphase Flows in Pipelines and Pipeline Networks.

Hei S.N., Wang K., Zheng C.X., Miao J.C., Huang Q.Y., 2023. Research on Determination Method of Low Temperature Gathering and Transportation Temperature of Dissolved Gas Crude Oil with High Water Cut. *Journal of Liaoning Petrochemical University*, 43(1): 32–37. DOI: 10.12422/j.issn.1672-6952.2023.01.006.

Huang J., Stoyanov S.R., Zeng H., 2019. A comparison study on adsorption and interaction behaviors of diluted bitumen and conventional crude oil on model mineral surface. *Fuel*, 253: 383–391. DOI: 10.1016/j.fuel.2019.05.011.

Joonaki E., Hassanpouryouzband A., Burgass R., Hase A., Tohidi B., 2020. Effects of waxes and the related chemicals on asphaltene aggregation and deposition phenomena: Experimental and modeling studies. *ACS Omega*, 5(13): 7124–7134. DOI: 10.1021/acsomega.9b03460.

Kouhi M., Shafiei A., Bekkuzhina T., Abutalip M., 2025. New intelligent models for predicting wax appearance temperature using experimental data – Flow assurance implications. *Fuel*, 380: 133146. DOI: 10.1016/j.fuel.2024.133146.

Li A., Zhu M.Q., Hao P.F., Wu H.H., Gong J., Wang K., Yu W.C., Feng Y.R., 2020. Wall sticking inhibition of high water cut crude oil (below pour point) by underwater superoleophobic PA-FC modification. *Colloids and Surfaces A: Physicochemical and Engineering Aspects*, 607: 125427. DOI: 10.1016/j.colsurfa.2020.125427.

Li B.F., Guo Z.Y., Li N., Wang D.X., Li G.H., Zheng L.M., Qi B., Jiao T.F., 2023. Molecular dynamics simulation of wax deposition in crude oil systems. *Colloids and Surfaces A: Physicochemical and Engineering Aspects*, 674: 131965. DOI: 10.1016/j.colsurfa.2023.131965.

Li B.F., Guo Z.Y., Zheng L.M., Shi E.X., Qi B., 2024. A comprehensive review of wax deposition in crude oil systems: Mechanisms, influencing factors, prediction and inhibition techniques. *Fuel*, 357: 129676. DOI: 10.1016/j.fuel.2023.129676.

Li X.L., Han W.C., Chen G.L., Yang M., Hu C.P., Shi H., Huang Q.Y., Lyu Y., 2022. Wall sticking behavior and adhesion theory of oil in low-temperature gathering and transportation by pipeline. *Oil & Gas Storage and Transportation*, 41(12): 1455–1463. DOI: 10.6047/j.issn.1000-8241.2022.12.012.

Li Y.X., 2010. Oil, gas and water multiphase flow in pipelines. *China University of Petroleum Press*. ISBN: 978-7-5636-3257-2.

Lin T., Gao H.S., Zhao S.H., Zeng K., Gong F., Yang W., 2022. Study and Application of Gathering and Transportation Limit at Low Temperature of Produced Fluid in Huabei Oilfield. [In:] *Proceedings of the 2021 International Petroleum and Petrochemical Technology Conference, Springer, Singapore*: 566–580. DOI: 10.1007/978-981-16-9427-1_54.

Liu J., Dong T., Lin D.C., Liang D.Q., 2024. Hydraulic–Thermal–Chemical Coupling Model Considering Hydrate Growth and Aggregation to Study the Hydrate Slurry Multiphase Flow in Oil–Water Systems. *Energy & Fuels*, 38(12): 10755–10765. DOI: 10.1021/acs.energyfuels.4c01357.

Lyu Y., Huang Q., Zhang F., Liu L., Zhang H., Zhang Y., Li R., Zhu X., Shi H., Zhang D., Wang Q., 2022a. Study on adhesion of heavy oil/brine/substrate system under shear flow condition. *Journal of Petroleum Science and Engineering*, 208: 109225. DOI: 10.1016/j.petrol.2021.109225.

Lyu Y., Huang Q.Y., Liu L.Q., Zhang D.X., Xue H.Y., Zhang F.Q., Zhang H.W., Li R.B., Wang Q.C., 2022b. Experimental and molecular dynamics simulation investigations of adhesion in heavy oil/water/pipeline wall systems during cold transportation. *Energy*, 250: 123811. DOI: 10.1016/j.energy.2022.123811.

Mydlarz-Gabryk K., Pietrzak M., Troniewski L., 2014. Study on oil–water two-phase upflow in vertical pipes. *Journal of Petroleum Science and Engineering*, 117: 28–36. DOI: 10.1016/j.petrol.2014.03.007

Nguyen D., Cao T., Pohl E., Russell C., Lucente-Schultz R., 2023. Investigation of asphaltene polydispersity, stability, and deposition on steel using XDLVO theory. *Energy & Fuels*, 38(10): 7314–7327. DOI: 10.1021/acs.energyfuels.3c00521.

Pham T., Truong H., Pham B., 2017. Flow Assurance in Subsea Pipeline Design for Transportation of Petroleum Products. *Open Journal of Civil Engineering*, 07: 311–323. DOI: 10.4236/ojce.2017.72021.

Qin Y., Wang Y., Huang Q., Wang K., Fei S., Zhong X., Liu W., Geng P., 2025. Investigation on the Safety Temperature Boundary After the Shutdown of Cold Transport Pipelines: Based on the XDLVO Theory and Force Balance. *Journal of Energy Resources Technology, Part B: Subsurface Energy and Carbon Capture*, 1(6): 061005. DOI: 10.1115/1.4069351.

Qin Y.Z., Zhang H.W., Yin R., Xiong J.H., Huang Q.Y., 2024. Method for determining temperature boundary of low temperature gathering and transportation of crude oil in extra-high water cut period. *Chemical Industry and Engineering Progress*, 43(10): 5475–5485. DOI: 10.16085/j.issn.1000-6613.2023-1643.

Rao Y., Liu Z., Wang S., Li L., 2022. Experimental Study on Hydrate Safe Flow in Pipelines under a Swirl Flow System. *ACS Omega*, 7(19): 16629–16643. DOI: 10.1021/acsomega.2c00892.

Shao B.L., Ren M., Tian N., 2024. Hourly natural gas load forecast based on STL-XGBoost-NBEATSx. *Journal of China University of Petroleum (Edition of Natural Science)*, 48 (No. 3): 170–179. DOI: 10.3969/j.issn.1673-5005.2024.03.019.

Sun X.S., Hou L., Yang K., Liu J.Q., Zhang X.R., Zhu Z.L., Tang S.S., Zhou Q.L., 2024. Simulation of flow characteristics of hydraulic suspension system of gelled crude oil based on population balance. *Journal of China University of Petroleum (Edition of Natural Science)*, 48(3): 162–169. DOI: 10.3969/j.issn.1673-5005.2024.03.018.

Sunday N., Settar A., Chetehouna K., Gascoin N., 2023. Numerical modeling and parametric sensitivity analysis of heat transfer and two-phase oil and water flow characteristics in horizontal and inclined flowlines using OpenFOAM. *Petroleum Science*, 20(2): 1183–1199. DOI: 10.1016/j.petsci.2022.10.008.

Wang Y.J., Huang Q.Y., Xu Z.K., Wei Z., Zhang X., Zhang Y., Liu W.C., Qi J.W., 2023. The investigation of flocculation and deposition of heavy components in the crude oil tank based on experiment and molecular simulation. *Fuel*, 353: 129217. DOI: 10.1016/j.fuel.2023.129217.

Xu P.Y., He L.M., Yang D.H., Zhou S., Wang J.W., Yang D., 2021. Blocking characteristics of high water-cut crude oil in low-temperature gathering and transportation pipeline. *Chemical Engineering Research and Design*, 173: 224–233. DOI: 10.1016/j.cherd.2021.07.019.

Yang D.H., Lu X.X., Liu S.J., Liang C.J., Han Y., Tan H., He L.M., 2022. Characteristics of low-temperature gathering of crude oil with high pour point and high viscosity in high water-cut period. *Oil & Gas Storage and Transportation*, 41(3): 311–317. DOI: 10.6047/j.issn.1000-8241.2022.03.009.

Yin X.Y., Li J., Shen J., Huang X.Y., Zhou F., Zhao Z.H., Su M., Dong X.J., Jing J.Q., Sun J., 2024. Study on the Flow Characteristics of Heavy Oil-Water Two-Phase Flow in the Horizontal Pipeline. *ACS Omega*, 9(23): 24396–24405. DOI: 10.1021/acsomega.4c00135.

Yu X., Gao Y.H., Cai D.J., Yao W., Zhou Y.W., Su Y.F., Liu K., 2021. Wax deposition law under a gas–liquid bubbly flow pattern. *ACS Omega*, 6(36): 23015–23022. DOI: 10.1021/acsomega.0c04911.

Zhang H.Q., Sarica C., Pereyra E., 2012. Review of High-Viscosity Oil Multiphase Pipe Flow. *Energy & Fuels*, 26(7): 3979–3985. DOI: 10.1021/ef300179s.

Zhang Y., Huang Q.Y., Cui Y., Li Q., Wang K., Su B.H., Lv Y., Li X.Y., Kong W.M., Shi H., Li W.D., 2020. Estimating wall sticking occurrence temperature based on adhesion force theory. *Journal of Petroleum Science and Engineering*, 187: 106778. DOI: 10.1016/j.petrol.2019.106778.

Zhao L., Zeng Q.S., Wang Z.M., 2018. Design and Performance of a Novel Autonomous Inflow Control Device. *Energy & Fuels*, 32(1): 125–131. DOI: 10.1021/acs.energyfuels.7b02673.

Zhou Q., Wei L., Li D., Wang L., Gao Y., 2025. Study on the unheated gathering boundaries of crude oil during high water content period in cold region. *Petroleum Science and Technology*, 43(17): 2392–2411. DOI: 10.1080/10916466.2024.2377349.

Zhou S.D., Guo Y., Lian M.M., Liu Y., Du H., Lv X.F., 2022. Study on the Adhesion Force between Wax Crystal Particles and Hydrate Particles. *ACS Omega*, 7(6): 5283–5291. DOI: 10.1021/acsomega.1c06458.

Zhu H.R., Li C.X., Yang F., Liu H.Y., Liu D.H., Sun G.Y., Yao B., Liu G., Zhao Y.S., 2018. Effect of thermal treatment temperature on the flowability and wax deposition characteristics of Changqing waxy crude oil. *Energy & Fuels*, 32(10): 10605–10615. DOI: 10.1021/acs.energyfuels.8b02552.

Zou X., Fu L.D., Wu L., Zuo W.H., 2023. Research on Multiphase Flow and Nozzle Wear in a High-Pressure Abrasive Water Jet Cutting Head. *Machines*, 11(6): 614. DOI: 10.3390/machines11060614.

Kexi LIAO, Professor
Petroleum Engineering School, Southwest Petroleum University
Chengdu, 610500, China

Huaixin ZHANG, Associate Professor
School of Computer Science and Software Engineering, Southwest Petroleum University
Chengdu, 610500, China
E-mail: *zhxswpi@163.com*

Guoxi HE, Associate Professor
Petroleum Engineering School, Southwest Petroleum University
Chengdu, 610500, China

Ziqi ZHANG, M.Sc. Student
Petroleum Engineering School, Southwest Petroleum University
Chengdu, 610500, China
E-mail: *1448072173@qq.com*

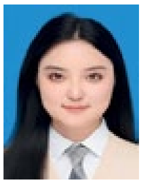

Min QIN, Lecturer
Petroleum Engineering School, Southwest Petroleum University
Chengdu, 610500, China

Tengjiao HE, Assistant Researcher
Petroleum Engineering School, Southwest Petroleum University
Chengdu, 610500, China
E-mail: *363272635@qq.com*

Yuhan LIU
Sichuan Natural Gas Sales Center, Sinopec Natural Gas Company
Chengdu, 610011, China